Screening EUV mask absorbers for defect repair

Takeshi Isogawa [a], Kazunori Seki [a], Mark Lawliss [b],
Emily Gallagher [b], Shinji Akima [a], Toshio Konishi [a]

[a]Toppan Photomasks Inc, 1000 River St., Essex Junction, VT 05452, USA
[b] IBM Microelectronics, 1000 River St., Essex Junction, VT 05452, USA

Phone: +1-802-769-8325 FAX: +1-802-769-5909 e-mail: takeshi.isogawa@toppan.co.jp

ABSTRACT

Five EUV film stacks were prepared and evaluated from the multiple viewpoints of mask repair process: etching property, CD control and wafer print. Etching property results revealed a thicker lower reflective (LR) layer stack showed good performance. Some types of defects were repaired and a CD comparison done with both CD-SEM and EUV microscope. It was found thinner total film stack (LR plus absorber) performs better than thicker ones for CD control. In addition, thicker LR performed better than thinner LR. Wafer print performance on the repaired site was evaluated through focus by imaging on an EUV microscope. Wafer printability performance showed that thinner total film stack performed better than a thicker one. Finally the best stack for EUV mask repair performance was determined to be a thinner total film stack and thicker a LR from all the various points of view.

Keywords: EUV, absorber stacks, mask defect repair, repairability, printability

1 INTRODUCTION

EUV (*Extreme Ultraviolet*) lithography is one of the most promising techniques for imaging 7-nm node wafer features. It is reported that the EUV absorber stack affects wafer printing performance and mask inspection performance. [1, 2] Several types of EUV absorber stack have been developed and are being evaluated. The impact on reparability of these film stacks has not yet reported. The most common method of EUV mask repair is etching with a combination of gas and electron beam. This method gives different results depending on target material and structure. In this study, five different EUV blanks were prepared. These blanks are evaluated from many viewpoints of the mask repair process. Then, we consider the relationship between EUV absorber stack and mask repairability.

2 METHODS

2.1 Materials

Figure 1 shows the EUV film structures used for this study. They are labeled Stack A, Stack B, Stack C, Stack D, and Stack E. All five stacks have same configuration from capping layer to the back side material: 2.5nm of Ru-capping layer, 40 pairs of Mo/Si bi-layers on the substrate and CrN on the back side. The difference among the stacks is the film height and composition of LR(low reflectivity layer) and absorber layer. Stack A has the thickest LR. Stack B, Stack C and Stack D have

Photomask and Next-Generation Lithography Mask Technology XXI, edited
by Kokoro Kato, Proc. of SPIE Vol. 9256, 92560N · © 2014 SPIE
CCC code: 0277-786X/14/$18 · doi: 10.1117/12.2070251

thinner LR with various absorber thickness. Stack B is the thinnest. Stack C's absorber is almost as thick StackA's. Stack D's absorber is the same thickness as Stack A's, but with thinner LR. Stack E's absorber is the thickest.

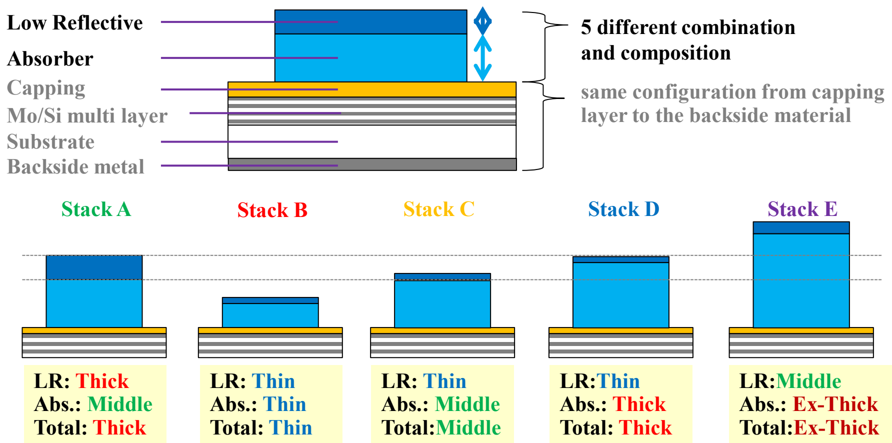

Figure 1. EUV film structures used for this study

2.2 Procedure

An EB (electron beam) repair tool was used for this analysis. As shown in Figure 2, the EB repair tool enables users to control exposure dose and repair region bias, which can control depth and width. In order to evaluate reparability, two types of programmed defects are evaluated. Programmed defects are designed and built with standard EB mask fabrication processes. Repair targets are a bridge on a 18nm(x1) LS (line and space) pattern and a missing hole on a 32nm(x1) array hole pattern shown in Figure 2.

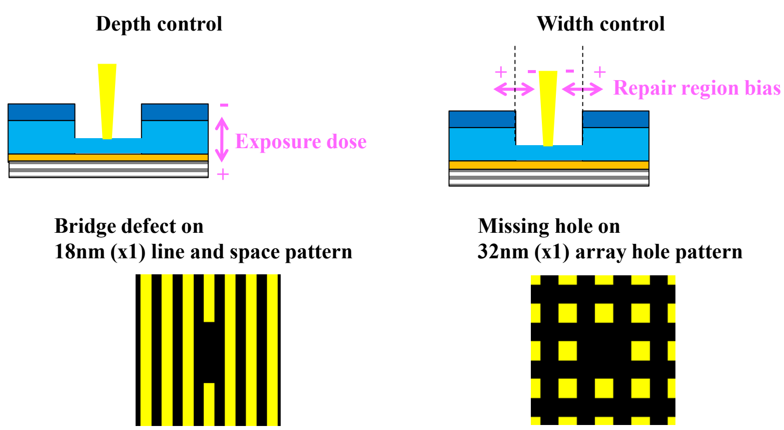

Figure 2. EB repair tool control (upper side) and programmed defects in this study

The repaired sites were measured for depth and width by with AFM, The critical dimension (CD) was measured on mask with a CD-SEM and with an EUV microscope. [3]

3 RESULTS AND DISCUSSIONS

3.1 Etching property (baseline assessment)

3.1.1 Etching rate

By controlling the etching rate, a difference caused by layer structures can be isolated and studied. We repaired a 500x500nm square area with varying dose. The repaired site was measured depth and half width by AFM. Figure 3 shows the etching rate of each stack. In the graph on left side, horizontal axis indicates dose and vertical axis indicates depth. All of stacks showed similar etching rate. In the graph on right side, the horizontal axis indicates dose and the vertical axis indicates half width. Stack A maintained a consistent trend along with dose. Stack C, Stack D, and Stack E tended to widen. Increasing width along with dose indicates it is easier to etch with higher exposure: there is more lateral etch. LR thickness prevents lateral etching.

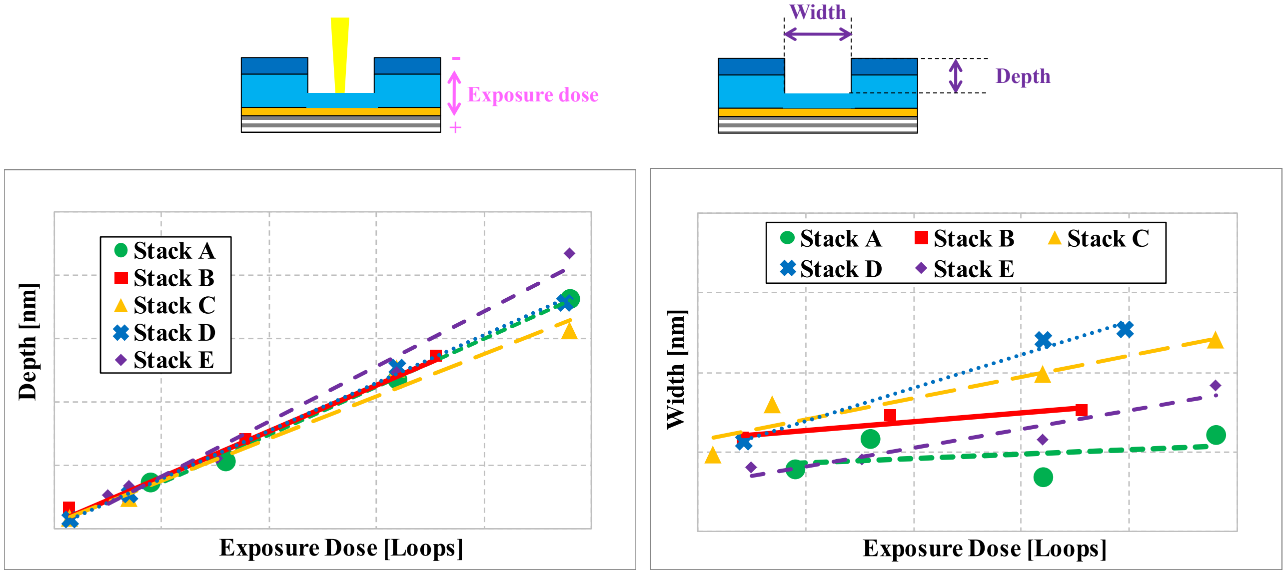

Figure 3. Etching rate results (Left: Depth rate, Right: Width rate)

3.2 Mask CD control (process optimization)

3.2.1 SEM images after repair

The repaired site shape is evaluated by comparing to other reference patterns. One of the most common methods is comparing the CD of reference sites to repaired sites. Repair condition such as dose and bias change the repaired site CD. Figure 4 shows SEM images of programmed defect repairs, one repaired site for each stack. Stack A and Stack B repaired shapes appear similar to reference shapes. Stack C, Stack D and Stack E repaired shapes appear broader than the reference shapes shown in both LS bridge and missing hole images. This trend might relate to LR and total film height.

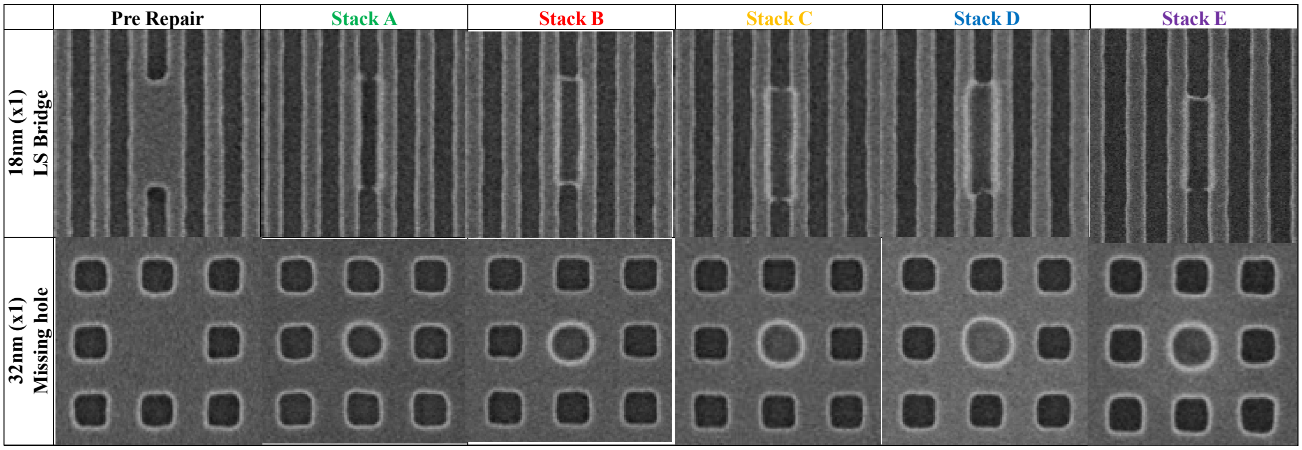

Figure 4. SEM images of programmed defect and repaired site on each stack

3.2.2 CD control by dose change

Too much dose could damage the film and cause a large CD error. This section investigates CD change as a function of dose change in order to compare the repair process margin of each stack. We repaired the programmed defects shown in Figure 2 with varying dose. Both reference CD and repaired site CD were measured with a CD-SEM. The CD difference between them was calculated in percent. Figure 5 shows the relationship between dose and delta CD change. The horizontal axis indicates dose change and the vertical axis indicates delta CD change. In order to see CD change, the 0% position is normalized for both in the horizontal and vertical. As shown in Figure 5, CD change vs. dose shows a similar trend; CD increases with increased dose and decreases with decreased dose. Therefore, the dose sensitivity of all stacks is similar.

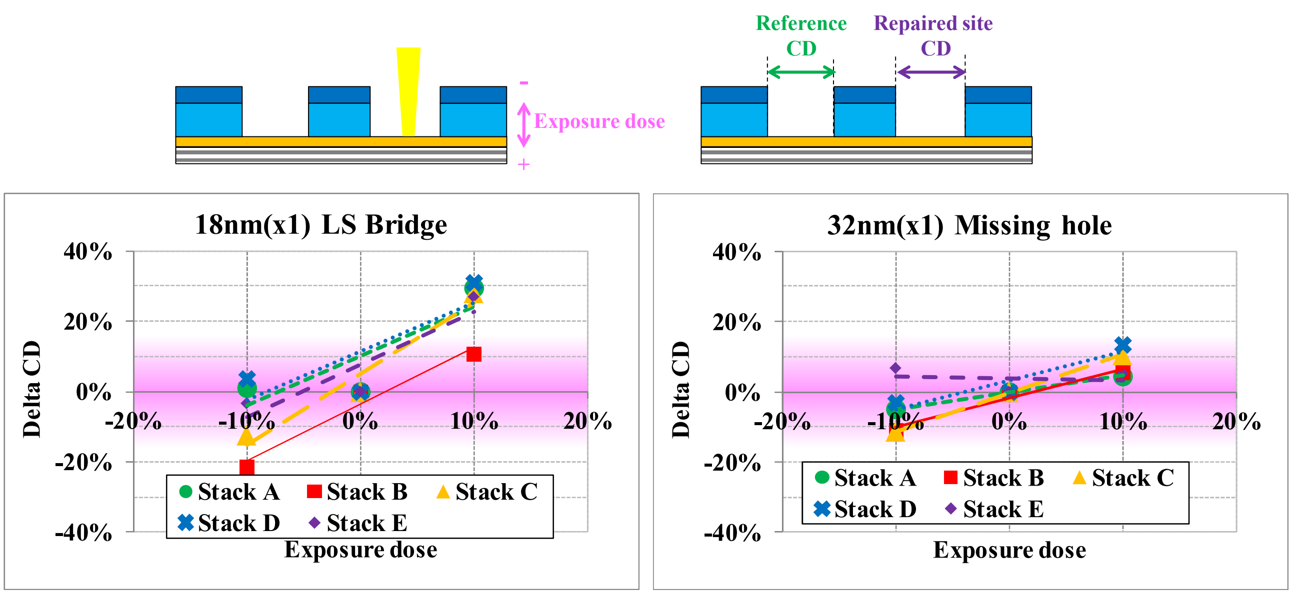

Figure 5. The relationship between dose and delta CD change (Left: LS bridge defect, Right: missing hole defect)

3.2.3 CD control by bias change

The bias parameter can control CD at the repaired site and lead to an optimized repair condition. This section investigates CD change vs. bias in order to see CD control on each stack. We implemented the same method as 3.2.2. . Figure 6 shows the relationship between bias and delta CD. The horizontal axis indicates bias offset value from standard and vertical axis indicates delta CD. Each graph has the specification criterion of plus or minus approximately 10% delta CD. The best stack performance maintains consistent delta CD closer to 0%. The acceptable stack performance is any parameter that stays within specification. On the other hand, a difficult stack to repair is outside of specification. In the case of a LS bridge repair, bias variation changed the repaired site CD drastically. In the case of the missing hole repair, bias variation was small, however the repaired site CD was higher than the reference CD. CD change was seen with bias change and approached delta 0% CD in Stack A, Stack B and Stack C. Stack D and Stack E didn't change CD and remained out of specification. Therefore, Stack A, Stack B and Stack C were acceptable for repair, however Stack D and Stack E were difficult to repair.

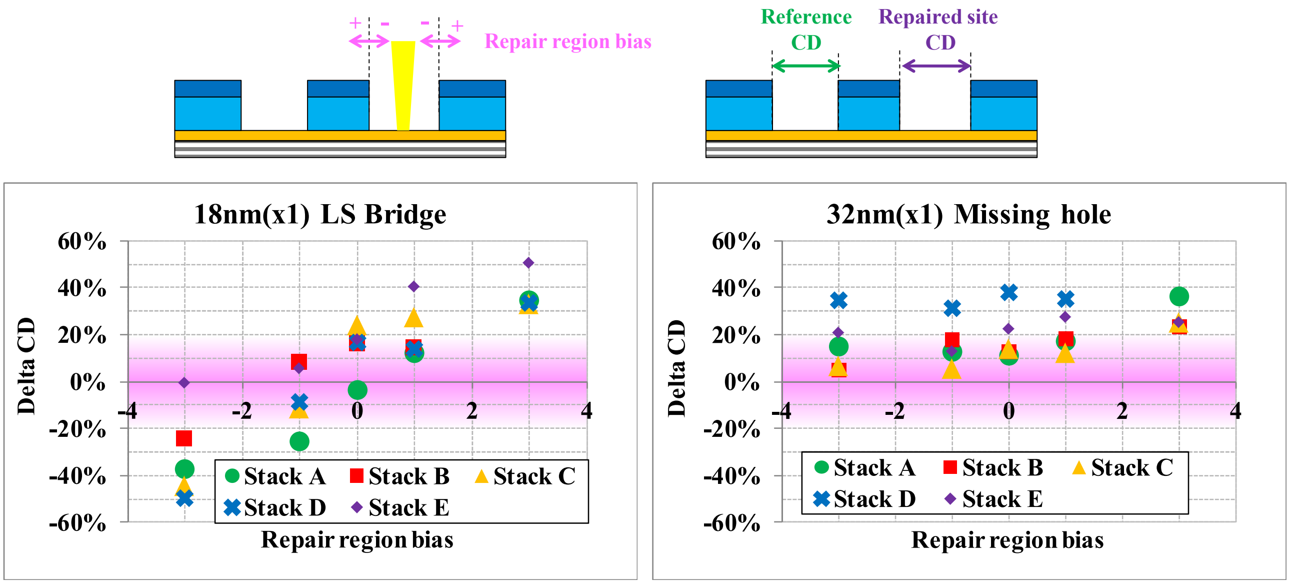

Figure 6. The relationship between bias and delta CD change (Left: LS bridge defect, Right: missing hole defect)

3.3 Wafer printability (stack performance comparison)

3.3.1 EUV microscope images after repair

The EUV microscope is able to observe patterns with an illumination condition which is equivalent to a current EUV scanner. Various wafer performance can be analyzed from the EUV microscope image. In terms of illumination settings aperture shapes were used depending on pattern types. Dipole shaped aperture was used for LS pattern: Quasar shaped aperture was used for array hole pattern: NA was 0.33 for both. Figure 7 shows EUV microscope images of programmed defect and repaired site on each stack. Each image was captured at best focus. As shown in Figure 7, we confirmed repaired site changed depending on repair condition. The middle row in each chart shows the results of optimized recipe, which was closest to 0% CD.

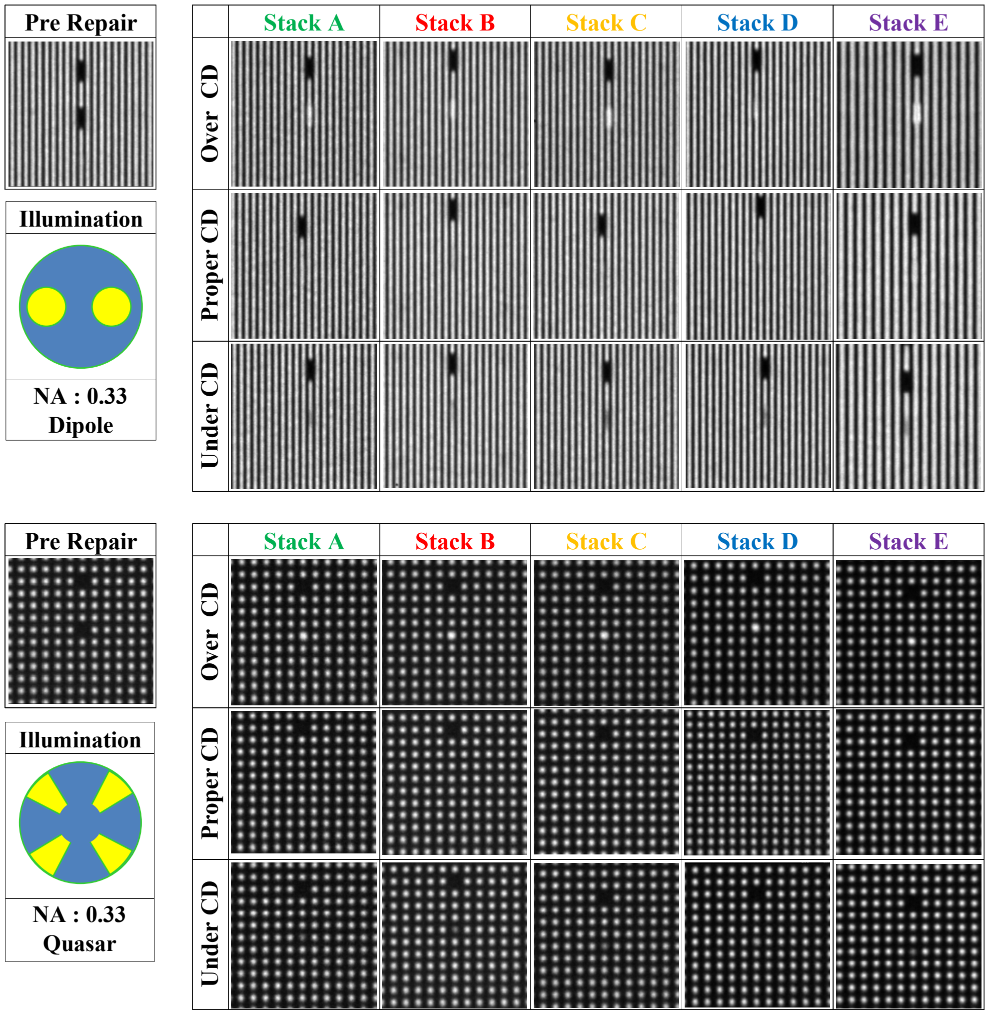

Figure 7. EUV microscope images of programmed defect and repaired site on each stack

3.3.2 Through-focus analysis

Through focus analysis was done to compare defect printability across all of the stacks. Programmed defects of the same size were analyzed with various steps of focus, and their printability was evaluated. Figure 8 shows the through focus evaluation results of repaired site on LS pattern and array hole patterns. Each repaired site was repaired with an optimum repair condition. The focus setting varied from -100 to +100nm. CD value at 0nm focus offset is normalized to the design width, which is 18nm in the LS pattern and 32nm in the array hole patterns. The graph enables us to see CD change at repaired site in response to the focus offset and to compare wafer performance for each stack. The amount of CD change at LS repaired site was a small in Stack A, Stack B and Stack C. Stack D and Stack E show larger CD change. The amount of CD change at the array hole repaired site is small in Stack B, Stack C and Stack D. Stack A is within the specification however variability is large. And, Stack E performed out of specification. Therefore, thinner film thickness should show better wafer performance based on actinic results. Using the same logic, thicker film thickness should show poorer wafer performance.

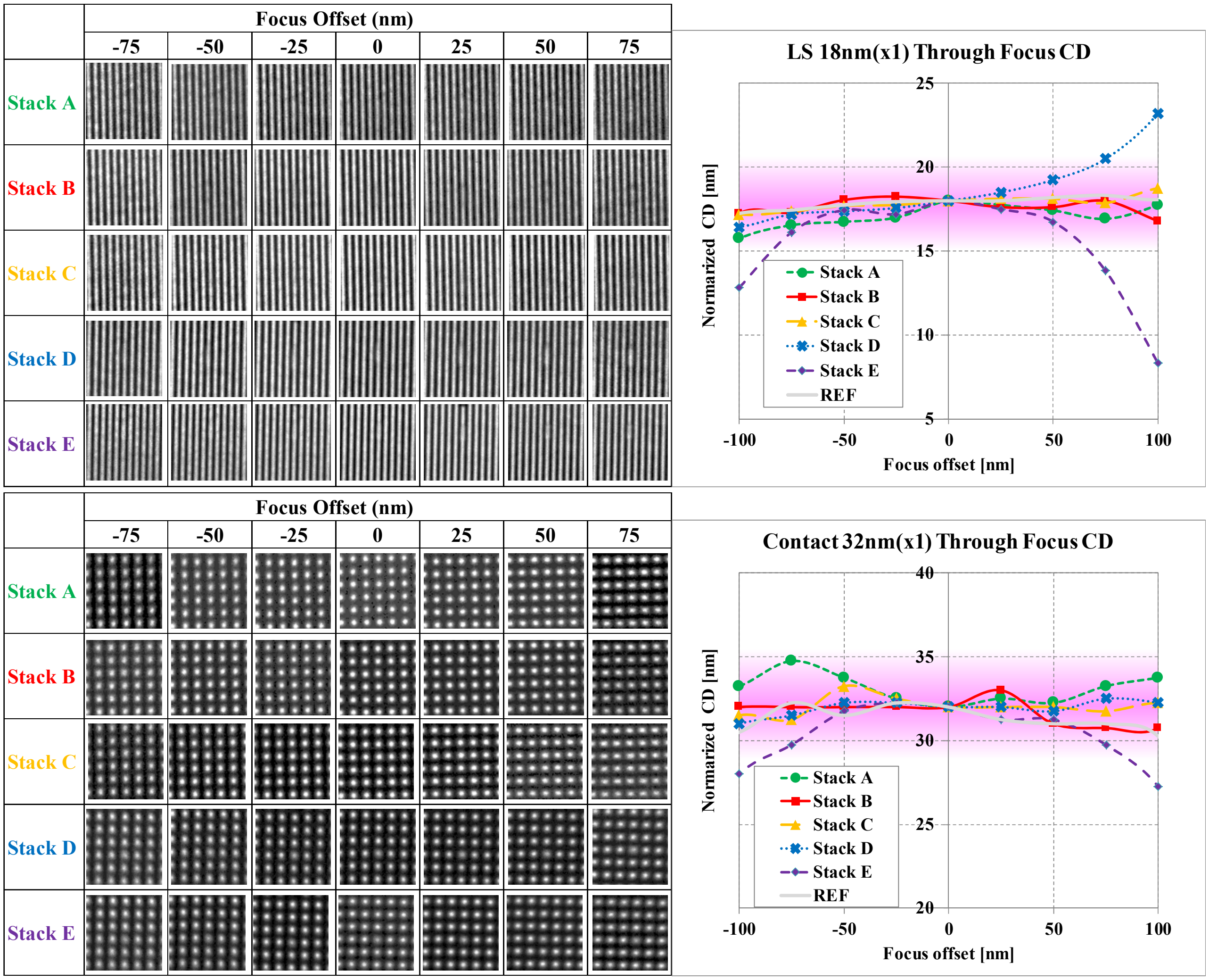

Figure 8. Through focus images of repaired site (on left) and CD change (on right)

3.4 The relationship between film thickness and repair performance

Generally thicker film stacks result in reduced CD control under various repair condition changes and performed worse for all repair characteristics. Stack A is the exception. Figure 9 describes the electron beam repair process. During electron beam exposure, the electrons scatter in the film during beam and affect the region surrounding the repair. The absorber is etched, not only in the vertical direction, but also in the lateral direction. When the thicker absorbers are etched, the dose increases until the beam reaches to the capping layer, so there is more time for lateral etching. It is easier to control the thinner absorber CD at the repaired site. Though Stack A and Stack D have the same total absorber film thickness, Stack A is easier to control with respect to CD and demonstrates good repair characteristics. The reason for the added control is that Stack A has thicker LR. Figure 10 shows the etching rate comparison of layers. The lateral etching is less effective in thicker LR layer, because the etching rate of LR is lower than that of the absorber.

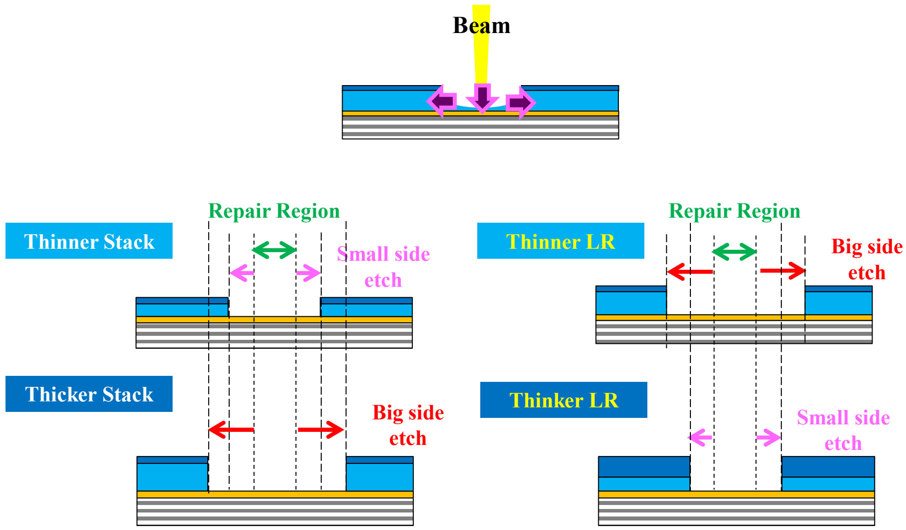

Figure 9. The mechanism of electron beam repair etching and the relationship between film thickness and lateral etching

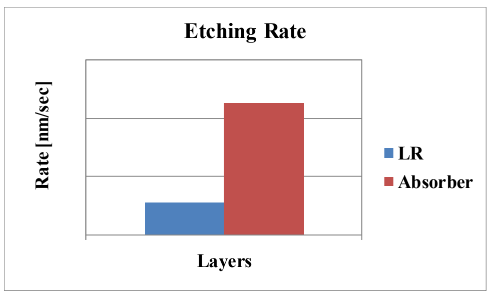

Figure 10. Etching rate comparison between LR and absorber

4 SUMMARY

Five films stacks were evaluated from various points of view as is documented in Table 1. In terms of etching property and CD control, Stack A, which has the thickest LR, performs best. Stack B and Stack C performed acceptably. Stack D and Stack E were difficult to repair. In terms of actinic imaging, Stack B and Stack C, whose films stack thicknesses, are relatively thin, performed well. Stack A, Stack D and Stack E, whose films stack thicknesses are thick, tended to perform poorly. In conclusion, the ideal film stack for the mask repair process has not only a thin total film thickness, but also thicker LR layer.

Table 1. Summary of this study

	Stack A	Stack B	Stack C	Stack D	Stack E
	LR:Thick Abs.: Middle Total:Thick	LR:Thin Abs.: Thin Total:Thin	LR:Thin Abs.: Middle Total:Middle	LR:Thin Abs.: Thick Total:Thick	LR:Middle Abs.: Ex-Thick Total:Ex-Thick
Etching property (Signal/Rate)	🙂	😐	😐	😐	☹️
CD controllability (Dose/Bias)	🙂	🙂	🙂	☹️	☹️
Wafer printability (Thru focus CD)	😐	🙂	🙂	☹️	☹️

🙂 **:Good**
😐 **:Acceptable**
☹️ **:Bad**

ACKNOWLEDGEMENTS

The authors would like to thank the following for their contributions to this paper: Kenneth Goldberg of Lawrence Berkeley National Laboratory and the SHARP (The SEMATECH High-NA Actinic Reticle review Project) team for EUV microscope imaging, Christopher Jarvis and Luke Bolton of IBM for AFM measurement and good discussions, Peter Bartlau and Robert Grego of IBM for mask handling, and Masayuki Kagawa of Toppan Photomask for fabricating mask. Finally we would like to thank the IBM and Toppan management and technical teams for support of this project.

REFERENCES

[1] Natalia Davydova et al., "Experimental approach to EUV imaging enhancement by mask absorber height optimization" Proc. SPIE 8166, 81663U (2011).

[2] Kazunori Seki et al., "Reflecting on inspectablity and wafer printability of EUV mask absorbers" Proc SPIE 8800, 88800S (2013).

[3] Kenneth A. Goldberg et al., "The SEMATECH high-NA actinic reticle review project (SHARP) EUV mask-imaging microscope" Proc. SPIE 8880, 88800T-1 (2013).